Anisotropic elasticity drives negative thermal expansion in monocrystalline SnSe

Ashoka Karunarathne,[1,2] Prakash Parajuli,[3] Gautam Priyadarshan,[4] Sriparna Bhattacharya,[3,*] Rahul Rao,[5] Pai-Chun Wei,[6,7] Yang-Yuan Chen,[6] Joseph R. Gladden,[1,2,†] and Apparao M. Rao[3,‡]

[1]*Department of Physics and Astronomy, University of Mississippi, University, Mississippi 38677, USA*
[2]*National Center for Physical Acoustics, University of Mississippi, University, Mississippi 38677, USA*
[3]*Clemson Nanomaterials Institute, Department of Physics & Astronomy, Clemson University, Clemson, South Carolina 29634, USA*
[4]*Department of Civil Engineering, University of Mississippi, University, Mississippi 38677, USA*
[5]*Air Force Research Laboratory, WPAFB, Ohio 45433, USA*
[6]*Institute of Physics, Academia Sinica, Taipei 11529, Taiwan, Republic of China*
[7]*Center for Condensed Matter Sciences and Center of Atomic Initiative for New Materials, National Taiwan University, Taipei 10617, Taiwan, Republic of China*

(Received 24 August 2020; revised 6 December 2020; accepted 5 January 2021; published 15 February 2021; corrected 29 September 2021)

Negative thermal expansion (NTE) materials have been at the center of attention for the past few decades as thermal expansion compensators in the fields of engineering, photonics, electronics, and medicine. Numerous crystalline materials exhibit NTE, wherein a combination of positive and negative linear thermal expansion coefficients results from their highly anisotropic elasticity. In this study, we selected SnSe, an anisotropic uniaxial NTE material as a model system where theoretical studies have linked its NTE along the *c* direction to transverse phonons and to positive Grüneisen parameters along all crystallographic axes. However, the fundamental origin of NTE in SnSe have not been experimentally resolved. Here we performed temperature-dependent resonant ultrasound spectroscopy (between 295–773 K) on single-crystalline SnSe to experimentally measure all nine independent elastic constants (C_{11}, C_{22}, C_{33}, C_{44}, C_{55}, C_{66}, C_{12}, C_{13}, C_{23}). Our data revealed a high degree of anisotropy in the temperature-dependent elastic constants with shear anisotropic factors show a contrasting pattern with increasing temperature. From this data we also deduced its material compressibility and negative Poisson's ratios in the major crystallographic directions that could explain its colossal linear thermal expansion coefficient along the *c* direction, reaching $\sim -12 \times 10^{-5}\,\mathrm{K}^{-1}$ at 773 K as reported in this study. Furthermore, we confirmed positive Grüneisen parameters along all the crystallographic axes and observe that SnSe behaves like a semicompressible parallelepiped with elastically coupled *a* and *b* axes, with the NTE being driven by the displacement of Sn atoms in the *c* direction.

DOI: 10.1103/PhysRevB.103.054108

I. INTRODUCTION

Interest in negative thermal expansion (NTE) materials dates back several centuries with the discovery of anomalous expansion of water between 0–4 °C. Since then, NTE has been well studied in a wide range of solid material systems, broadly classified as conventional and phase-transition-type materials [1], with the vision of creating zero expansion composite materials for future applications [2,3]. Of particular interest is the study of NTE in anisotropic crystalline materials, where a combination of positive and negative linear thermal expansion coefficients result from a highly anisotropic elasticity. Single crystalline SnSe is one such anisotropic chalcogenide, and has received considerable attention in recent years due to its surprisingly low thermal conductivity and high thermoelectric figure of merit [4–12]. The intrinsically low thermal conductivity is driven by a strong lattice anharmonicity owing to its unique anisotropic crystal structure. SnSe has a layered orthorhombic (*Pnma* below transition temperature, $T_c \sim 810\,\mathrm{K}$) crystal structure at room temperature with each layer composed of strongly bonded two-atom thick Sn-Se [along the *bc* plane; Fig. 1(a)] slabs that are stacked along the *a* direction (with weaker Sn-Se bonding).

Previous temperature-dependent neutron scattering measurements indicate that SnSe exhibits NTE along one of its crystallographic directions at $T < T_c$, *viz.*, the bond length along its *c* direction decreases with increasing temperature in the *Pnma* phase [9,13]. Theoretical calculations [14,15] suggest the NTE to be driven by bond rotations and the phonon modes transverse to the *c* axis. The NTE materials are also typically associated with negative axial Grüneisen parameters, $\gamma_i = -\frac{\partial \ln \omega}{\partial \varepsilon_i}$ (where ε_i is the strain along the i^{th} direction), which is a direct measure of the relationship between the phonon frequency ω and crystal volume change. However, for SnSe, discrepancies exist in the literature, with both positive and negative values reported experimentally [14] and theoretically [7,14,15] for the Grüneisen parameter (γ_3) along the *c* direction. In this regard, Bansal *et al.* [14] is the only group that reported the Grüneisen parameters using a combination of experimental and computational elastic constants to arrive at the conclusion that Grüneisen parameter is negative along

*Corresponding author: bbhatta@g.clemson.edu
†Corresponding author: jgladden@olemiss.edu
‡Corresponding author: arao@clemson.edu

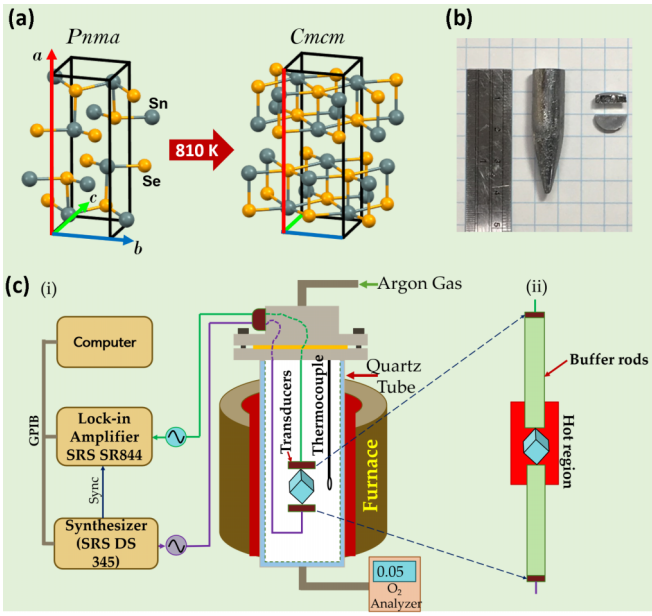

FIG. 1. Sample crystal structure and experimental setup. (a) Crystal structures of the *Pnma* and *Cmcm* phases of SnSe below and above the phase transition $T_c \sim 810$ K. (b) Single crystalline SnSe bulk sample and (c) RUS experimental setup with (i) direct contact transducer system for measurements up to 800 K, and (ii) buffer rod transducer system for measurements up to 1200 K.

the c direction, which contradicts all theoretical calculations including their own DFT calculation.

Nonetheless, the origins of NTE in SnSe have yet to be explored fully experimentally. The inconsistencies in the reported values of Grüneisen parameter may be attributed to a lack of understanding of the complex relationship between the various directional Grüneisen parameters γ_i and the anisotropic elastic properties of the SnSe crystal [16]. Hence, a complete knowledge of the temperature-dependent elastic constants of SnSe is essential to accurately determine the magnitude and sign of γ_i. To this end, we measured the elastic stiffness tensor (C_{ij}) of single-crystalline SnSe using the resonant ultrasound spectroscopy (RUS) in the temperature range 300–800 K. Our RUS data revealed a high degree of anisotropy in the temperature-dependent elastic constants, confirming a positive γ_3 in the temperature range ($\sim$ 295–725 K) despite its NTE along the c direction, which is consistent with the reported DFT calculations [15].

II. EXPERIMENTAL METHODS

A. Sample preparation

High-quality single crystalline SnSe samples [Fig. 1(b)] (packing density >99% of the theoretical density) were synthesized by the Bridgman method at the Institute of Physics, Academia Sinica, Taiwan [9]. The as-grown SnSe crystals were cleaved along the a direction and the in-plane orientation of SnSe single crystals were explicitly identified by x-ray diffraction phi-scans. Subsequently, the crystal was cut along the three major crystallographic directions to the size of $2.024 \times 3.531 \times 4.775\,\text{mm}^3$ (± 0.001 mm) for RUS measurements.

B. High-temperature resonant ultrasound spectroscopy (RUS)

RUS is a precise and efficient method, which uses a measured resonance spectrum to determine the elastic stiffness tensor of crystalline solids [17–20]. In contrast to other conventional nondestructive acoustical techniques, RUS is capable of measuring the elasticity constants at higher temperatures up to $\sim$ 1200 K depending on the robustness of its transducers at high temperature [Fig. 1(c)] [21–24]. In RUS, the resonance spectrum of a polished rectangular parallelepiped shaped crystalline sample is measured by exciting it with a swept-frequency continuous wave (CW) mode over a fixed frequency range, and the sample response to the excitation is detected by $LiNbO_3$ acoustic transducers, which are in-contact with the sample [Fig. 1(c-i)]. An iterative procedure that entails the crystal geometry and density is used to match the experimental frequencies with the calculated spectrum, which then allows determination of all elastic constants of the sample from a single frequency scan [17,19]. However, for high-temperature RUS measurements above 800 K, the transducers must be isolated from the sample by acoustic rods to protect the transducers from deteriorating from exposure to high temperature [Fig. 1(c-ii)].

In this study, resonance spectra of the sample were measured at elevated temperatures from 295–773 K using a direct contact transducer system made with $LiNbO_3$ piezoelectric transducers, placed inside a sealed glass tube, which is housed in a tube furnace. Elastic stiffness tensors at different temperature points were computed from the measured resonance frequencies in the spectra and the sample specification data. We used the thermal expansion coefficients described in Fig. 4(a) to calculate the dimensions of sample at the elevated temperatures and those updated dimensions were used in elastic constants fitting routine. In this nine-elastic constant optimization algorithm, a guided fitting routine was followed to prevent weakly coupled elastic constants from varying dramatically. The change of a natural frequency with respect to a change in each of the elastic constants ($\partial f_k/\partial C_{ij}$) varies significantly. Thus, the nine elastic constants were set into groups of three to vary (or float) in each fitting routine. The most significant (largest derivatives) elastic constants C_{44}, C_{55}, C_{66} were varied first, followed with varying the next group of C_{11}, C_{22}, C_{33}, until the final group of C_{12}, C_{13}, C_{23} was varied. Then the optimized elastic constants were used as the initial fit parameters in the fitting routine at next temperature.

Theoretically calculated (DFT) elastic constants by Li *et al.* [25] were used as initial parameters in the fitting routine. In a nonlinear optimization algorithm, it is important to make sure that it is settled in a global minimum rather than a local minimum. To ensure that the results were optimized at a global minimum, 20 different fittings were performed by using the randomly varied initial fit parameters such that their standard deviations were within $\pm 5\%$ of the initial DFT values. In this way, 20 optimized values for each elastic constant at each temperature were observed and their averages were taken as the final temperature-dependent elastic constants as shown in Figs. 2(a)–2(c). The uncertainty bars represent the standard deviations of the 20 optimized values of each elastic constant [26].

Computed elastic constants were then used to determine the temperature dependence of the macroscopic elastic

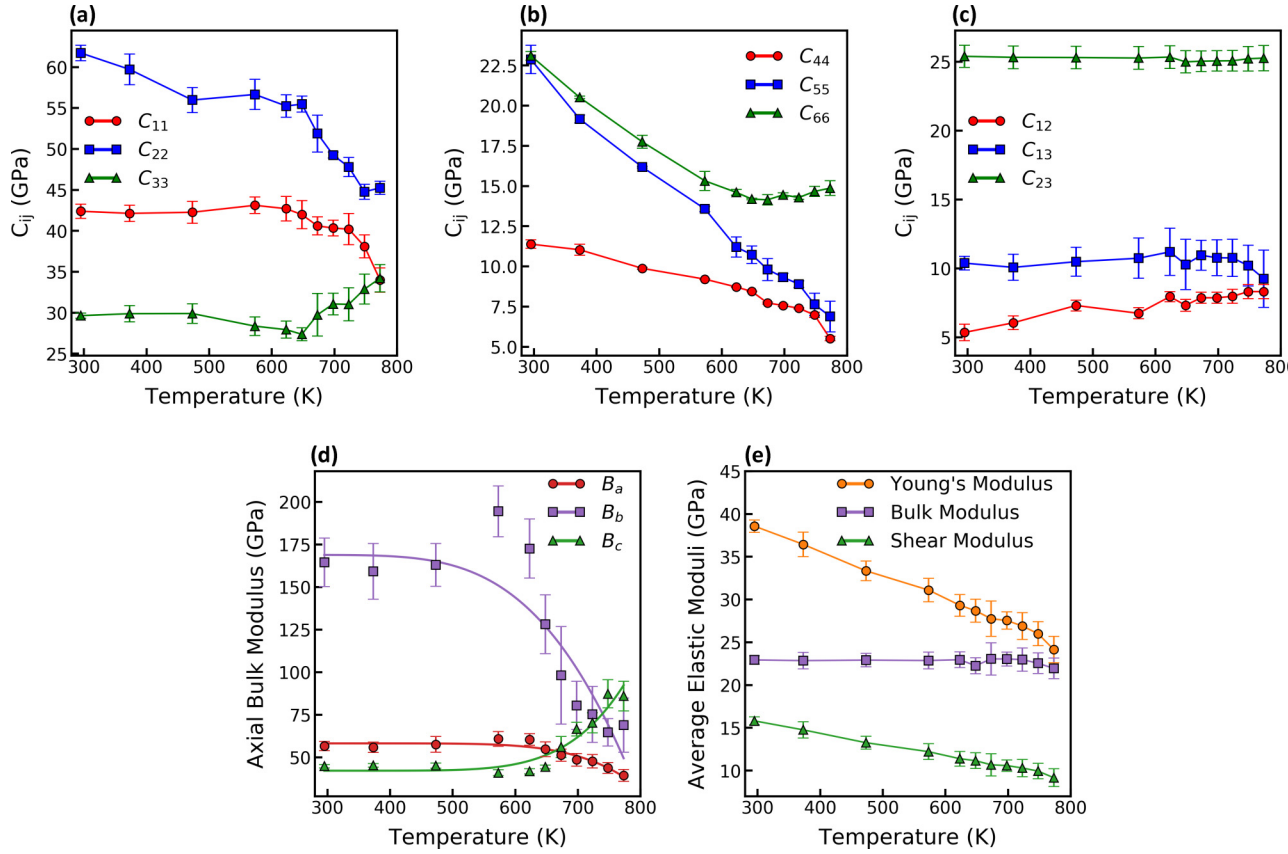

FIG. 2. Elastic constants and moduli of SnSe. Temperature-dependent (a) extensional, (b) shear, and (c) off-diagonal elastic constants (the error bars represent the standard deviations of 20 different fitting routines), (d) axial bulk moduli (fitted with the empirical Varshni function [30] to elicit their temperature dependence, and (e) Young's modulus, bulk modulus, and shear modulus.

moduli, axial bulk moduli, and shear anisotropic factors. Due to the limitation of maximum operating temperature of the direct contact transducer system, typically ∼800 K for $LiNbO_3$, a buffer rod transducer system was used to measure resonance spectra up to 953 K in order to detect the change in elastic constants across T_c. [27,28] Due to the acoustical losses through the long buffer rods, all resonance peaks were not observed in the measured spectra. Therefore, instead of computing elastic constants, trends in the temperature-dependent resonance frequencies were used as indicators for T_c [26]. It should be mentioned that all high-temperature data were collected under flowing Ar gas (low oxygen environment) to protect the samples from oxidation.

III. RESULTS AND DISCUSSION

According to harmonic theory, the potential energy (U) of the lattice vibrations is limited to the quadratic term of the interatomic displacements, and the elastic constants are temperature independent [29]. However, for crystal lattices that exhibit temperature-dependent elastic constants, the higher-order cubic and quartic terms in U corresponding to the anharmonic three- and four-phonon decay processes, respectively, must also be taken into account [29,30]. Elasticity, a measure of material response to applied stress or strain fields, is often used to determine the properties of lattice vibrations, thermal transport mechanisms, and structural arrangements within crystal structures. The relation between the stress tensor σ_{ij} and strain tensor ε_{kl} is given by the generalized Hooke's law as, $\sigma_{ij} = c_{ijkl}\varepsilon_{kl}$ [31–33]. The proportionality parameter c_{ijkl} is referred to the fourth rank elastic stiffness tensor with 81 elements. The symmetry of the stress and strain tensors reduces the indices $ijkl$ into a two-index form of ij using the Voigt convention, such that c_{ijkl} simplifies to C_{ij} a second rank 6×6 matrix with 36 elements. The number of independent elements, called elastic constants, are reduced into 21 (for triclinic symmetry) due to the symmetry relation $C_{ij} = C_{ji}$. The number of nonzero independent elastic constants are further reduced by the crystallographic symmetries of the crystalline materials [21]. For example, there are nine independent elastic constants of SnSe owing to its orthorhombic crystal symmetry, and its elastic tensor can be written as follows,

$$C_{ij} = \begin{pmatrix} C_{11} & C_{12} & C_{13} & 0 & 0 & 0 \\ C_{12} & C_{22} & C_{23} & 0 & 0 & 0 \\ C_{13} & C_{23} & C_{33} & 0 & 0 & 0 \\ 0 & 0 & 0 & C_{44} & 0 & 0 \\ 0 & 0 & 0 & 0 & C_{55} & 0 \\ 0 & 0 & 0 & 0 & 0 & C_{66} \end{pmatrix}. \quad (1)$$

The elastic potential energy density (U) can be expanded in terms of strain tensor as [34,35]

$$U = \frac{1}{2!}\sum_{ijkl} C_{ijkl}\varepsilon_{ij}\varepsilon_{kl} + \frac{1}{3!}\sum_{ijklmn} C_{ijklmn}\varepsilon_{ij}\varepsilon_{kl}\varepsilon_{mn} + \cdots . \tag{2}$$

Within the harmonic approximation, the higher-order terms in U can be neglected and represented by only the quadratic part in Eq. (2).

The variations of the measured elastic constants with increasing temperature from 295–773 K are illustrated in Figs. 2(a)–2(c), grouping them into extensional, shear, and off-diagonal terms. According to the statics of the elastic constant fitting procedure, the average of the uncertainties of the extensional constants (C_{11}, C_{22}, C_{33}) was found to be ∼1.5% at room temperature and it has increased to ∼3.7% at 773 K. Similarly, the uncertainty of shear constants (C_{44}, C_{55}, C_{66}) has increased from ∼1.8–2.8% and that of weakly coupled off-diagonal constants (C_{12}, C_{13}, C_{23}) has increased from ∼6.4–10.7% at the elevated temperature. The observed increase of uncertainties is possibly due to the uncertainties associated with resonance frequency measurements at higher temperatures. The accuracy of resonance frequency measurements is mainly reduced by the low Q factor. For example, single crystalline SnSe exhibits an intrinsic acoustical energy loss due to its strong lattice anharmonicity, which leads to a low Q factor (∼500 at $T = 295$ K) in the resonance spectrum and it is further reduced by the thermoelastic energy loss mechanism at the elevated temperatures (∼250 at $T = 773$ K).

Notably, the elastic constants C_{44}, C_{55}, C_{66}, which represent the shear modes, exhibit a dramatic reduction down to ∼35–70% of their room temperature values. The off-diagonal elastic constants C_{23}, and C_{13} has followed a slow reduction down to 1–10%, while C_{12} follows a rapid increase up to 55% from the room temperature values. The extensional mode constants C_{11} and C_{22} except C_{33} reduce between 19–27% of their room temperature values, indicating the softening of the extensional modes along the *a*- and *b*-crystallographic directions near the critical temperature. When compared to the variations of other elastic constants, C_{33} exhibits an increase of ∼16% near the phase transition temperature, indicating the stiffening of the extensional mode along the *c* direction. This observed deviation of C_{33} from the other extensional elastic constants can be rationalized from the calculated temperature-dependent axial bulk moduli B_a, B_b, B_c along *a, b,* and *c* direction respectively [Fig. 2(d)], where B_i is defined as the inverse of the linear compressibility, which provides the rigidity of the material extension (or compression) along the i^{th} direction due the applied volumetric stress (or pressure) [36,37]. In contrast, the extensional elastic constant C_{ii} ($i = 1, 2, 3$) represents the rigidity of the material extension (or compression) along i^{th} direction due to the applied stress along the same i^{th} direction. The axial bulk moduli were calculated according to the following:

$$B_a = \frac{\chi}{1+\alpha+\beta}, \quad B_b = \frac{B_a}{\alpha}, \quad B_c = \frac{B_a}{\beta}, \tag{3}$$

where,

$$\chi = C_{11} + 2C_{12}\alpha + C_{22}\alpha^2 + 2C_{13}\beta + C_{33}\beta^2 + 2C_{23}\alpha\beta \tag{4}$$

$$\alpha = \frac{(C_{11}-C_{12})(C_{33}-C_{13}) - (C_{23}-C_{13})(C_{11}-C_{13})}{(C_{33}-C_{13})(C_{22}-C_{12}) - (C_{13}-C_{23})(C_{12}-C_{23})} \tag{5}$$

$$\beta = \frac{(C_{22}-C_{12})(C_{11}-C_{13}) - (C_{11}-C_{12})(C_{23}-C_{12})}{(C_{22}-C_{12})(C_{33}-C_{13}) - (C_{12}-C_{23})(C_{13}-C_{23})}. \tag{6}$$

It is clear from Fig. 2(d) that the calculated bulk modulus along the *c* direction, B_c increases near T_c, while B_a and B_b decrease with temperature. This variation of the axial bulk moduli illustrates the softening of the extensional modes along the *a* and *b* directions and stiffening along the *c* direction as the temperature increases towards T_c. The observed higher value of B_b in the low temperature is due to the high stiffness along the *b* direction, which is also confirmed by the higher value of C_{22} than the other extensional elastic constants. The above observations can be related to the change of the crystal structure and lattice constants between the room temperature *Pnma* phase to the high-temperature *Cmcm* phase [13]. At T_c, the weak Sn-Se bond along the *c* direction in the *Pnma* phase [Figs. 1(a) and 3(b)] becomes stronger due to the displacive phase transition to *Cmcm* phase, resulting a reduction of the lattice constant from 4.439–4.293 Å. This bond reinforcement is consequently observed as an increase of both C_{33} and B_c with increasing temperature [Figs. 2(a) and 2(d)] [13,15].

Due the elastic anisotropic behavior of SnSe, the Voigt-Reuss-Hill (VRH) approximation was used to convert the anisotropic elastic constants to the macroscopic elastic moduli, which represent the average (effective) elasticity of the crystalline material [12,36,37]. According to the Voigt assumption the bulk (B_V) and the shear moduli (G_V) are expressed as:

$$B_V = \tfrac{1}{9}(C_{11} + C_{22} + C_{33} + 2C_{12} + 2C_{13} + 2C_{23}) \tag{7}$$

$$G_V = \tfrac{1}{15}(C_{11} + C_{22} + C_{33} - C_{12} - C_{13} - C_{23} + 3C_{44} + 3C_{55} + 3C_{66}). \tag{8}$$

From the Reuss approximation these moduli can be expressed as,

$$B_R = \frac{1}{(S_{11}+S_{22}+S_{33}) + 2(S_{12}+S_{13}+S_{23})} \tag{9}$$

$$G_R = \frac{15}{4(S_{11}+S_{22}+S_{33}) - 4(S_{12}+S_{13}+S_{23}) + 3(S_{44}+S_{55}+S_{66})}, \tag{10}$$

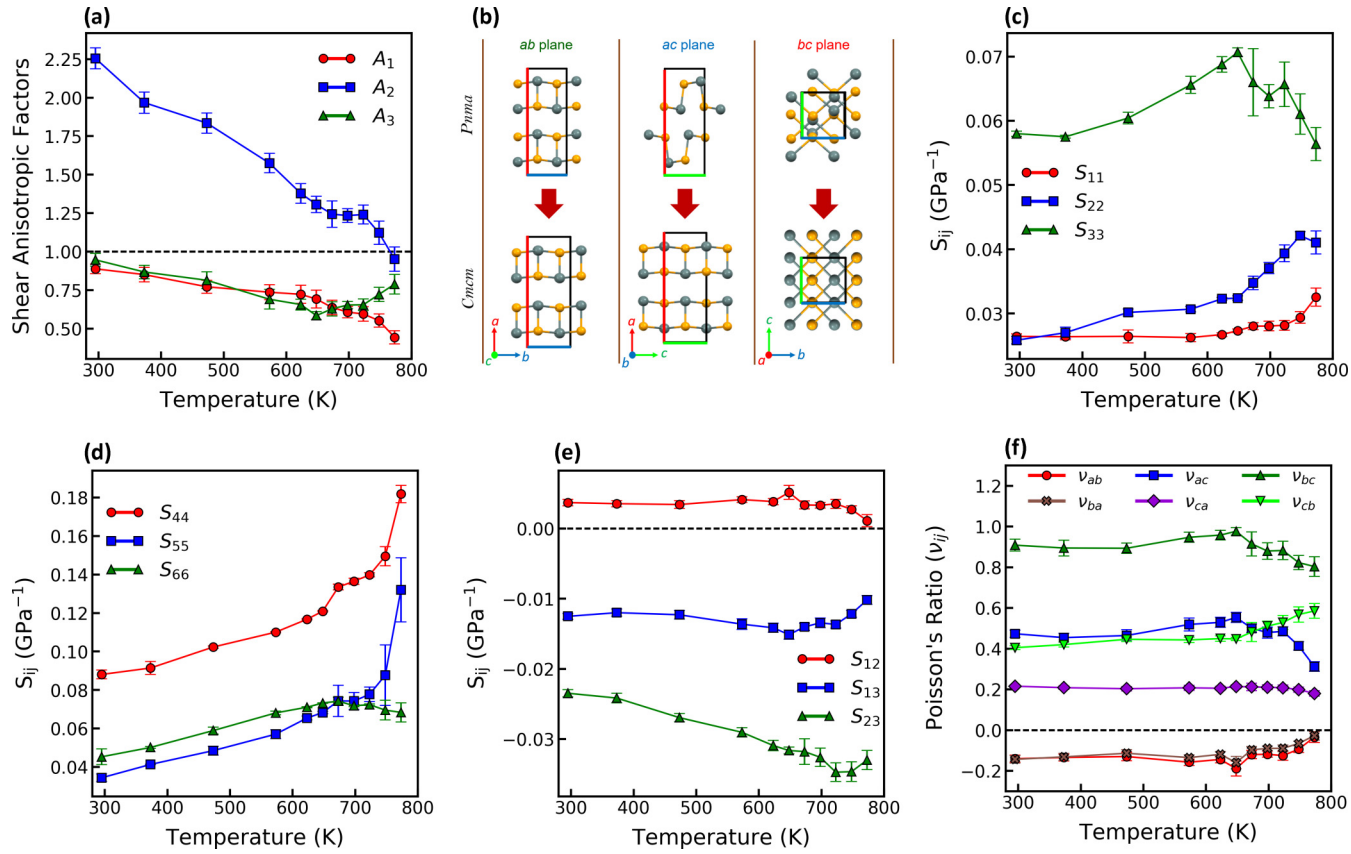

FIG. 3. Elastic anisotropy in SnSe. Temperature-dependent (a) shear isotropic factors, (b) a schematic of crystallographic planes of SnSe as the crystal transitions from the *Pnma* to the *Cmcm* phase, (c)–(e) elastic compliance constants, and (d) Poisson's ratio.

where, $[S_{ij}] = [C_{ij}]^{-1}$ where S_{ij} represents the components of elastic compliance tensor. The Voigt equations represent the upper limit of the polycrystalline constants while Reuss equations represent the lower limit. Therefore, the elastic moduli can be approximated by Hill's average and hence the bulk modulus, shear modulus, and Young's modulus can be expressed as $B = \frac{(B_V+B_R)}{2}$, $G = \frac{(G_V+G_R)}{2}$, and $E = \frac{9BG}{3B+G}$, respectively. The calculated elastic moduli decrease with increasing temperature, showing an overall material softening with increasing temperature before the phase transition point [Fig. 2(e)].

The macroscopic elastic anisotropy of SnSe is more clearly demonstrated by the shear anisotropic factors (A_i), which illustrate the anisotropy in the bond dynamics between atoms at the nanoscale in the different planes of the SnSe [Fig. 3(a)]. The shear anisotropic factors are defined as follows: (i) $A_1 = 4C_{44}/(C_{11} + C_{33} - 2C_{13})$ for the {100} plane between ⟨011⟩ and ⟨010⟩ directions, (ii) $A_2 = 4C_{55}/(C_{22} + C_{33} - 2C_{23})$ for the {010} plane between ⟨101⟩ and ⟨001⟩ directions, and (iii) $A_3 = 4C_{66}/(C_{11} + C_{22} - 2C_{12})$ for the {001} plane between ⟨110⟩ and ⟨010⟩ directions [36]. The crystal planes become elastically isotropic when the $A_i = 1$, and any departure from unity is an indicator of elastic anisotropy in the planes. Interestingly, the shear anisotropic factor A_2, which corresponds to the *ac* plane reaches 1 at 773 K from 2.3 at 300 K, indicating an increasing elastic isotropy in the *ac* plane up to T_c [Fig. 3(a)]. This shift in A_2 can be clearly understood from the different crystallographic planes as SnSe transitions from the *Pnma* to the *Cmcm* phase. These differences are shown schematically in Fig. 3(b). Indeed, the *ac* plane below T_c is clearly the most distorted plane compared to the other planes of SnSe within which the Sn atom (initially bonded to the Se atom only along one direction) develops a new Sn-Se bond that leads to more isotropic bonding characteristics in the *Cmcm* phase. This anisotropic-to-isotropic shift in the *ac* plane is reflected by the most prominent change in the value of A_2. In contrast, relatively subtle transitions in the bonding characteristics of the *bc* and *ab* planes are observed across T_c that are reflected by the subtle shifts in the values of A_1 and A_3, respectively.

Recently, based on DFT calculations, Hong and Delaire deduced that the strong anharmonicity of SnSe originates from the chemical instability of the in-plane resonant bonding through a spontaneous Jahn-Teller-like distortion [38]. Based on prior neutron diffraction experiments by Chattopadhyay *et al.* [13], it is well known that SnSe exhibits a second-order displacive phase transition where a continuous movement of Sn atoms along the *c* direction is the order parameter of the phase transition. This relative movement of Sn atoms partially utilizes the thermal energy provided to the crystal, which in turn proportionally deprives the crystal from expanding along the *c* direction. This movement of the Sn atoms with increasing temperature also leads to the elastic anisotropy along different crystallographic directions [as revealed by the

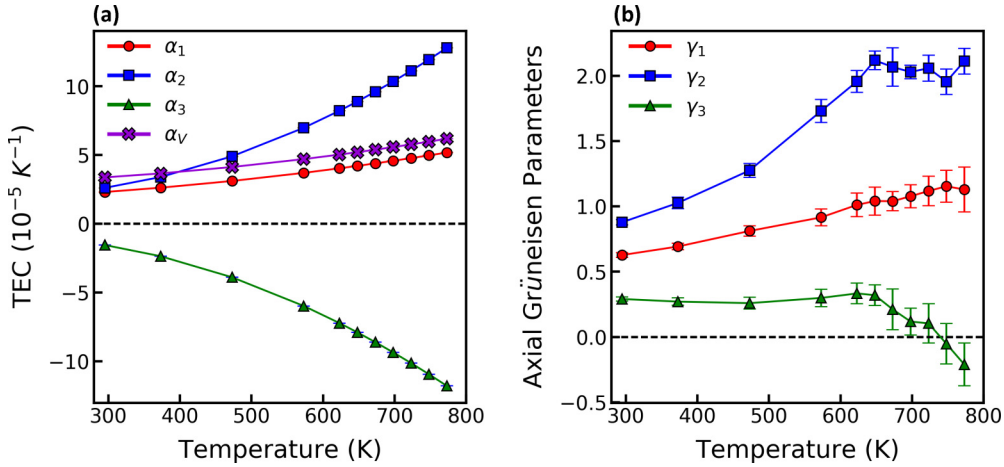

FIG. 4. Temperature-dependent crystal expansion. Temperature-dependent (a) thermal expansion coefficients obtained from the temperature-dependent XRD reported in a previous study [9], and (b) the axial Grüneisen parameters of SnSe from the thermal expansion coefficients and RUS data [see Eqs. (13)–(15)].

elasticity constants in Figs. 2(a)–2(c)] and at the same time, acts as the source of the nonlinear force constant along c axis [38].

The elastic anisotropy in SnSe is further illustrated by plotting the elastic compliance constants, which are shown in Figs. 3(c)–3(e). The elastic compliance constants ($S_{ij} = \frac{\partial \epsilon_i}{\partial \sigma_j}$) are defined as the amount of strain developed in the i^{th} direction due to a unit stress in the j^{th} direction [29]. Equation (11) describes how SnSe behaves when stress is applied along different directions to the crystal, where the "<" or ">" relationships reflect the trends shown in Figs. 3(c)–3(e).

$$\begin{bmatrix} S_{11} = \frac{\partial \epsilon_1}{\partial \sigma_1} > 0 & S_{12} = \frac{\partial \epsilon_1}{\partial \sigma_2} > 0 & S_{13} = \frac{\partial \epsilon_1}{\partial \sigma_3} < 0 \\ S_{21} = \frac{\partial \epsilon_2}{\partial \sigma_1} > 0 & S_{22} = \frac{\partial \epsilon_2}{\partial \sigma_2} > 0 & S_{23} = \frac{\partial \epsilon_2}{\partial \sigma_3} < 0 \\ S_{31} = \frac{\partial \epsilon_3}{\partial \sigma_1} < 0 & S_{32} = \frac{\partial \epsilon_3}{\partial \sigma_2} < 0 & S_{33} = \frac{\partial \epsilon_3}{\partial \sigma_3} > 0 \end{bmatrix}. \quad (11)$$

The S_{ij} relationships shown in Eq. (11) clearly show that the SnSe crystal behaves like a semicompressible parallelepiped with two coupled ac and bc planes (coupled a and b axes). For example, looking at the first column in Eq. (11), if SnSe is compressed along the a direction, it will expand along the c direction and shrink along the a and b directions. This behavior arises from the anisotropy in the bond elasticity between atoms along different crystallographic directions [Figs. 3(c)–3(e)], which is further supported by the temperature-dependent directional Poisson's ratios. The directional Poisson's ratios $\nu_{ij} = -\frac{S_{ij}}{S_{ii}}$, defined as the ratio of lateral contraction along j^{th} direction to longitudinal extension along i^{th} direction, are derived from the elastic compliance constants and their temperature dependencies are shown in Fig. 3(f). The negative values of ν_{ab} (and ν_{ba}) imply expansion of the lattice along b (a) direction due the applied strain along a (b) direction. The lattice compresses along the c direction with the applied strain along a (or b) direction consistent with the above explanation.

The components of the elastic compliance tensor S_{ij} are also related to the thermal expansion coefficients (TECs) α_l of the anisotropic SnSe crystal within the quasiharmonic approximation as follows: [15]

$$\alpha_l = \frac{C_V}{V_0} \sum_k S_{lk} \gamma_k, \quad (12)$$

where, γ_k are the Grüneisen parameters that provide a quantitative link between the thermal and mechanical parameters of solids [39]. Figure 4(a) shows the temperature dependence of the TECs along the three crystallographic directions calculated using the temperature-dependent lattice constants from a prior study, [9] where the volumetric TEC, α_V can be obtained by $\alpha_V = \alpha_1 + \alpha_2 + \alpha_3$. The TECs along the a and b directions (α_1, α_2) are positive and increase with temperature while the TEC along the c direction (α_3) is negative across the entire temperature range, reaching a very high value of $\sim -12 \times 10^5\ K^{-1}$ at 773 K.

The thermal expansion of a solid is mainly determined by two factors: a strain-dependent entropy producing thermal pressure quantified by the Grüneisen parameter γ_k, and the elastic response to that thermal pressure measured by the material compressibility, K defined by $K_i = \sum_{k=1}^{3} S_{ik}$ [40,41]. When considering the thermodynamics and structural change of the SnSe crystal, γ_k is often used to estimate the strength of the lattice anharmonicity as it is a direct measure of the relationship between the phonon frequency and crystal volume change. Using these experimentally determined α_l values [9] [Fig. 4(a)], we obtained the temperature-dependent γ_k using the relation $\gamma_k = \frac{V_0}{C_V} \sum_l C_{kl} \alpha_l$, and the results are plotted in Fig. 4(b). Contrary to the expectation of negative Grüneisen parameters, we see that γ_1 and γ_2 are positive from room temperature until the phase transition, while γ_3 is positive between 295–725 K and becomes negative close to the phase transition. The crossover of γ_3 from a positive value to a negative value above 725 K is attributed to (i) the fact that quasiharmonic approximation (because of a lack of anharmonic model) is involved in Eqs. (12)–(15) while the actual crystal system becomes strongly anharmonic at temperatures nearing T_c, and to some extent (ii) the uncertainty involved in the measurement of elastic constants at higher temperatures. A slight decrease in γ_2 can also be seen above 650 K, and

can be attributed to the two shortcomings described above. Equation (12) can be expanded as:

$$\alpha_1 = \frac{C_V}{V_0}[S_{11}\gamma_1 + S_{12}\gamma_2 + S_{13}\gamma_3] > 0 \quad (13)$$

$$\alpha_2 = \frac{C_V}{V_0}[S_{12}\gamma_1 + S_{22}\gamma_2 + S_{23}\gamma_3] > 0 \quad (14)$$

$$\alpha_3 = \frac{C_V}{V_0}[S_{13}\gamma_1 + S_{23}\gamma_2 + S_{33}\gamma_3] < 0. \quad (15)$$

It is noteworthy that both Eqs. (13) and (14) both contain one negative term (i.e., S_{13} and S_{23}, respectively) whereas Eq. (15) contains both S_{13} and S_{23}. The negative values of S_{13} and S_{23} directly result in the large negative TEC along the c direction, and consequently observed NTE along the c direction. The NTE brings the Sn and Se atoms closer together, which leads to a stiffening of the bonds between the Sn and Se atoms. Thus, bond stiffening along the c direction explains both the unusual increase in C_{33} (which is defined as the amount of stress developed along the c direction due to a unit strain along the c direction, i.e., $C_{33} = \frac{\partial \sigma_3}{\partial \epsilon_3}$) and the axial bulk modulus B_c with increasing temperature. This result confirms that the negative thermal expansion can be achieved even with positive Grüneisen parameters, which has been reported in previous theoretical studies [15,16].

IV. CONCLUSIONS

The nine independent elastic constants of SnSe, a low symmetry crystal structure, were measured using RUS in the temperature range ~300–800 K. The anisotropy in the elastic properties is clearly evident in the marked decrease of the shear constants with increasing temperature as well as the increase of the axial bulk modulus along the c axis. These effects also result in negative Poisson's ratios and a large linear negative thermal expansion coefficient along the c direction of the SnSe crystal. Furthermore, the temperature-dependent Grüneisen parameters were found to be positive along all crystal directions. Taken together, our RUS measurements explain the origin of NTE in SnSe and emphasize the role of elastic anisotropy in the properties of this unique material.

[1] K. Takenaka, Front. Chem. **6**, 1 (2018).

[2] J. Chen, F. Wang, Q. Huang, L. Hu, X. Song, J. Deng, R. Yu, and X. Xing, Sci. Rep. **3**, 2458 (2013).

[3] C. K. Gan, J. R. Soh, and Y. Liu, Phys. Rev. B **92**, 235202 (2015).

[4] L.-D. Zhao, G. Tan, S. Hao, J. He, Y. Pei, H. Chi, H. Wang, S. Gong, H. Xu, V. P. Dravid, C. Uher, G. J. Snyder, C. Wolverton, and M. G. Kanatzidis, Science **351**, 141 (2016).

[5] C. Chang, M. Wu, D. He, Y. Pei, C.-F. Wu, X. Wu, H. Yu, F. Zhu, K. Wang, Y. Chen, L. Huang, J.-F. Li, J. He, and L.-D. Zhao, Science **360**, 778 (2018).

[6] A. T. Duong, V. Q. Nguyen, G. Duvjir, V. T. Duong, S. Kwon, J. Y. Song, J. K. Lee, J. E. Lee, S. Park, T. Min, J. Lee, J. Kim, and S. Cho, Nature Commun. **7**, 13713 (2016).

[7] L.-D. Zhao, S.-H. Lo, Y. Zhang, H. Sun, G. Tan, C. Uher, C. Wolverton, V. P. Dravid, and M. G. Kanatzidis, Nature (London) **508**, 373 (2014).

[8] P.-C. Wei, S. Bhattacharya, J. He, S. Neeleshwar, R. Podila, Y. Y. Chen, and A. M. Rao, Nature (London) **539**, E1 (2016).

[9] P.-C. Wei, S. Bhattacharya, Y.-F. Liu, F. Liu, J. He, Y.-H. Tung, C.-C. Yang, C.-R. Hsing, D.-L. Nguyen, C.-M. Wei, M.-Y. Chou, Y.-C. Lai, T.-L. Hung, S.-Y. Guan, C.-S. Chang, H.-J. Wu, C.-H. Lee, W.-H. Li, R. P. Hermann, Y.-Y. Chen, and A. M. Rao, ACS Omega **4**, 5442 (2019).

[10] R. K. Vankayala, T. Lan, P. Parajuli, F. Liu, R. Rao, S. H. Yu, T. Hung, C. Lee, S. Yano, C. Hsing, D. Nguyen, C. Chen, S. Bhattacharya, K. Chen, M. Ou, O. Rancu, A. M. Rao, and Y. Chen, Adv. Sci. **7**, 2002494 (2020).

[11] F. Liu, P. Parajuli, R. Rao, P. C. Wei, A. Karunarathne, S. Bhattacharya, R. Podila, J. He, B. Maruyama, G. Priyadarshan, J. R. Gladden, Y. Y. Chen, and A. M. Rao, Phys. Rev. B **98**, 224309 (2018).

[12] A. Karunarathne, J. R. Gladden, G. Priyadarshan, P.-C. Wei, T.-L. Hung, P. Parajuli, S. Bhattacharya, Y.-Y. Chen, and A. M. Rao, ACS Appl. Energy Mater. **1**, 6123 (2018).

[13] T. Chattopadhyay, J. Pannetier, and H. G. Von Schnering, J. Phys. Chem. Solids **47**, 879 (1986).

[14] D. Bansal, J. Hong, C. W. Li, A. F. May, W. Porter, M. Y. Hu, D. L. Abernathy, and O. Delaire, Phys. Rev. B **94**, 054307 (2016).

[15] G. Liu, J. Zhou, and H. Wang, Phys. Chem. Chem. Phys. **19**, 15187 (2017).

[16] E. T. Ritz and N. A. Benedek, Phys. Rev. Lett. **121**, 255901 (2018).

[17] A. Migliori, J. L. Sarrao, W. M. Visscher, T. M. Bell, M. Lei, Z. Fisk, and R. G. Leisure, Phys. B Condens. Matter **183**, 1 (1993).

[18] A. Migliori and J. D. Maynard, Rev. Sci. Instrum. **76**, 121301 (2005).

[19] A. Migliori and J. L. Sarrao, *Resonant Ultrasound Spectroscopy: Applications to Physics, Materials Measurements, and Nondestructive Evaluation* (J. Wiley, New York, 1997).

[20] B. J. Zadler, J. H. L. Le Rousseau, J. A. Scales, and M. L. Smith, Geophys. J. Int. **156**, 154 (2004).

[21] G. Li and J. R. Gladden, Int. J. Spectrosc. **2010**, 206362 (2010).

[22] S. Bhattacharya, A. Mehdizadeh Dehkordi, S. Tennakoon, R. Adebisi, J. R. Gladden, T. Darroudi, H. N. Alshareef, and T. M. Tritt, J. Appl. Phys. **115**, 223712 (2014).

[23] S. Tennakoon, Y. Peng, M. Mookherjee, S. Speziale, G. Manthilake, T. Besara, L. Andreu, and F. Rivera, Sci. Rep. **8**, 1372 (2018).

[24] A. Karunarathne, K. S. Jodha, G. Priyadarshan, J. A. Griggs, and J. R. Gladden, J. Am. Ceram. Soc. **103**, 1312 (2020).

[25] G. Li, U. Aydemir, M. Wood, W. A. Goddard, P. Zhai, Q. Zhang, and G. J. Snyder, Chem. Mater. **29**, 2382 (2017).

[26] See Supplemental Material at http://link.aps.org/supplemental/10.1103/PhysRevB.103.054108 for the temperature-dependent elastic constants of SnSe measured by RUS, temperature-dependent mean sound velocity and the phonon relaxation times of selected vibrational modes of SnSe, and temperature-dependent resonance frequency trend across the phase transition temperature Tc, which includes Refs. [42–48].

[27] A. Sather, J. Acoust. Soc. Am. **43**, 1291 (1968).
[28] C. K. Jen, L. Piche, and J. F. Bussiere, J. Acoust. Soc. Am. **88**, 23 (1990).
[29] C. Kittel, *Introduction to Solid State Physics* (Wiley, New York, 1996).
[30] Y. P. Varshni, Phys. Rev. B **2**, 3952 (1970).
[31] A. E. H. Love, *A Treatise on the Mathematical Theory of Elasticity* (University Press, Cambridge, 1927).
[32] I. S. Sokolnikoff, *Mathematical Theory of Elasticity* (McGraw-Hill, New York, 1946).
[33] S. Timoshenko and J. N. Goodier, *Theory of Elasticity*, 3rd ed. (McGraw-Hill, New York, 1969).
[34] H. Wang and M. Li, Phys. Rev. B **79**, 224102 (2009).
[35] D. C. Wallace, Am. J. Phys. **40**, 1718 (1972).
[36] P. Ravindran, L. Fast, P. A. Korzhavyi, B. Johansson, J. Wills, and O. Eriksson, J. Appl. Phys. **84**, 4891 (1998).
[37] Y. Wen, L. Wang, H. Liu, and L. Song, Cryst. **7**, 39 (2017).
[38] J. Hong and O. Delaire, Mater. Today Phys. **10**, 100093 (2019).
[39] F. D. Stacey and J. H. Hodgkinson, Phys. Earth Planet. Inter. **286**, 42 (2019).
[40] R. W. Munn, J. Phys. C Solid State Phys. **5**, 535 (1972).
[41] A. B. Cairns and A. L. Goodwin, Phys. Chem. Chem. Phys. **17**, 20449 (2015).
[42] G. A. Slack and S. Galginaitis, Phys. Rev. **133**, A253 (1964).
[43] D. Wang and G. Wang, Phys. Lett. A **381**, 801 (2017).
[44] H. Ledbetter and A. Migliori, J. Appl. Phys. **100**, 063516 (2006).
[45] H. R. Chandrasekhar, R. G. Humphreys, U. Zwick, and M. Cardona, Phys. Rev. B **15**, 2177 (1977).
[46] J. M. Skelton, L. A. Burton, S. C. Parker, A. Walsh, C.-E. Kim, A. Soon, J. Buckeridge, A. A. Sokol, C. R. A. Catlow, A. Togo, and I. Tanaka, Phys. Rev. Lett. **117**, 075502 (2016).
[47] X. Xu, Q. Song, H. Wang, P. Li, K. Zhang, Y. Wang, K. Yuan, Z. Yang, Y. Ye, and L. Dai, ACS Appl. Mater. Interfaces **9**, 12601 (2017).
[48] S. Bhattacharya, D. C. Marinescu, J. R. Morris, I. A. Sergienko, B. Sales, D. Mandrus, and V. Keppens, Phys. Rev. B **86**, 024402 (2012).

Correction: A misspelled name in the first sentence of the 8th paragraph of Sec. III has been corrected.